Effects of spin-orbit coupling on the optical response of a material

Tae Yun Kim,[1] Andrea Ferretti,[2] and Cheol-Hwan Park[1,*]

[1]*Department of Physics, Seoul National University, Seoul 08826, Korea*
[2]*Centro S3, CNR-Istituto Nanoscienze, 41125 Modena, Italy*

We investigate the effects of spin-orbit coupling on the optical response of materials. In particular, we study the effects of the commutator between the spin-orbit coupling part of the potential and the position operator on the optical matrix elements using density functional theory calculations within the generalized gradient approximation. By means of a formalism that separates a fully relativistic Kleinman-Bylander pseudopotential into the scalar-relativistic and spin-orbit-coupling parts, we calculate the contribution of the commutator arising from spin-orbit coupling to the squared optical matrix elements of isolated atoms, monolayer transition-metal dichalcogenides, and topological insulators. In the case of isolated atoms from H ($Z = 1$) to Bi ($Z = 83$), the contribution of spin-orbit coupling to the squared matrix elements can be as large as 14%. On the other hand, in the cases of monolayer transition-metal dichalcogenides and topological insulators, we find that this contribution is less than 1% and that it is sufficient to calculate the optical matrix elements and subsequent physical quantities without considering the commutator arising from spin-orbit coupling.

I. INTRODUCTION

The electronic structure of materials containing heavy elements can be significantly affected by spin-orbit coupling (SOC). Due to the recent advances in the investigation of materials having strong SOC effects, such as transition-metal dichalcogenides (TMDCs), topological insulators, or Weyl semimetals, to name a few, it becomes important to accurately simulate the effects of SOC using first-principles density functional theory (DFT) calculations. Because SOC allows the manipulation of the spin degrees of freedom in materials by using light [1–6], understanding the effects of SOC on the optical response of materials is a matter of importance.

Consider a system described by an effective Hamiltonian,

$$\hat{H} = \frac{\hat{\mathbf{p}}^2}{2m} + V_{\text{loc}}(\hat{\mathbf{r}}) + \hat{V}_{\text{NL}}, \tag{1}$$

where m is the mass of an electron, $\hat{\mathbf{p}}$ is the momentum operator, $\hat{\mathbf{r}}$ is the position operator, and $V_{\text{loc}}(\hat{\mathbf{r}})$ and $\hat{V}_{\text{NL}}$ are the local and nonlocal parts of the potential, respectively. The optical matrix elements of the system are given by the matrix elements of the velocity operator [7]

$$\hat{\mathbf{v}} = \frac{\hat{\mathbf{p}}}{m} + \frac{i}{\hbar} [\hat{V}_{\text{NL}}, \hat{\mathbf{r}}]. \tag{2}$$

In many DFT calculations, the pseudopotential method is used because of its computational efficiency. Within the nonrelativistic and scalar-relativistic pseudopotential methods, the effects of the commutator in Eq. (2) on the optical matrix elements and absorption spectra have been investigated

for various types of systems, such as isolated atoms [8], semiconductors [9], and metals [10]. It was reported that the contribution of the commutator can be large, e.g., as in the cases of a carbon atom [8] and bulk copper [10].

SOC is proportional to $\hat{\mathbf{L}} \cdot \hat{\mathbf{S}}$, where $\hat{\mathbf{L}}$ and $\hat{\mathbf{S}}$ are the orbital and spin angular momentum operators, respectively. Because the orbital angular momentum operator does not commute with the position operator, SOC results in an additional contribution to the velocity operator via the commutator and to the optical matrix elements.

It has not been well established whether the effects of the commutator arising from the SOC part of the potential are important or not in a system where the influence of SOC on the electronic structure is known to be strong. For example, in some previous studies on the optical response of Bi_2Se_3, a topological insulator that has been extensively investigated, the contribution of the commutator arising from SOC was neglected, and $\hat{\mathbf{p}}/m$ as an approximation to $\hat{\mathbf{v}}$ [Eq. (2)] was used to calculate the optical matrix elements [5,6,11]. On the other hand, the authors of a recent study [12] on the circular dichroism of Bi_2Te_3 claimed that the SOC contribution to the velocity operator plays a crucial role in explaining the results of their photoemission experiments.

In this study, we investigate the effects of SOC on the optical matrix elements and absorption spectra in various types of systems: isolated atoms, monolayer TMDCs, and topological insulators. The method used in this study allows for the calculation of the optical matrix elements with and without inclusion of the commutator arising from the intrinsic nonlocality of SOC while using the same (fully relativistic) pseudopotential, from which we can directly assess the importance of the effects of SOC in evaluating the optical matrix elements and optical properties of materials.

*cheolhwan@snu.ac.kr

II. METHODS

The nonlocal part of a fully relativistic pseudopotential in semilocal form can be written as [13]

$$\hat{V}_{\text{SL}} = \sum_{l=0}^{l_{\max}} \sum_{j=|l-\frac{1}{2}|}^{l+\frac{1}{2}} \sum_{m_j=-j}^{j} |l, j, m_j\rangle V_{l,j}(r) \langle l, j, m_j|, \quad (3)$$

where $V_{l,j}(r)$ is the radial potential of $\hat{V}_{\text{SL}}$ for a given pair of the orbital angular momentum quantum number l and the total angular momentum j, and $|l, j, m_j\rangle$ is the spin-angular function [14] satisfying $\hat{\mathbf{J}}^2|l, j, m_j\rangle = j(j+1)\hbar^2|l, j, m_j\rangle$ and $\hat{J}_z|l, j, m_j\rangle = m_j\hbar|l, j, m_j\rangle$ ($\hat{\mathbf{J}} = \hat{\mathbf{L}} + \hat{\mathbf{S}}$).

The spin-angular function can be explicitly written in terms of the orbital angular momentum eigenstates $|l, m_l\rangle$ satisfying $\hat{\mathbf{L}}^2|l, m_l\rangle = l(l+1)\hbar^2|l, m_l\rangle$ and $\hat{L}_z|l, m_l\rangle = m_l\hbar|l, m_l\rangle$ ($m_l = -l, \ldots, l$) and the spin-angular momentum eigenstates $|\uparrow\rangle$ and $|\downarrow\rangle$: for $j = l + 1/2$,

$$|l, j, m_j\rangle = \sqrt{\frac{l + m_j + \frac{1}{2}}{2l + 1}} \left| l, m_j - \frac{1}{2} \right\rangle |\uparrow\rangle$$

$$+ \sqrt{\frac{l - m_j + \frac{1}{2}}{2l + 1}} \left| l, m_j + \frac{1}{2} \right\rangle |\downarrow\rangle, \quad (4)$$

and for $j = |l - 1/2|$,

$$|l, j, m_j\rangle = \sqrt{\frac{l - m_j + \frac{1}{2}}{2l + 1}} \left| l, m_j - \frac{1}{2} \right\rangle |\uparrow\rangle$$

$$- \sqrt{\frac{l + m_j + \frac{1}{2}}{2l + 1}} \left| l, m_j + \frac{1}{2} \right\rangle |\downarrow\rangle. \quad (5)$$

Using the fact that the spin-angular function is an eigenstate of $\hat{\mathbf{L}} \cdot \hat{\mathbf{S}}$, $\hat{V}_{\text{SL}}$ can be rewritten as the sum of the scalar-relativistic and SOC parts [13,15]:

$$\hat{V}_{\text{SL}} = \sum_{l=0}^{l_{\max}} |l\rangle V_l^{\text{SR}}(r) \langle l| + \sum_{l=1}^{l_{\max}} |l\rangle V_l^{\text{SO}}(r) \hat{\mathbf{L}} \cdot \hat{\mathbf{S}} \langle l|, \quad (6)$$

where $|l\rangle\langle l|$ is the orbital angular momentum projector for a given l, which is the sum of $|l, m_l\rangle\langle l, m_l|$ over all m_l. In Eq. (6), the radial potentials of the scalar-relativistic and SOC parts of $\hat{V}_{\text{SL}}$ are given as

$$V_l^{\text{SR}}(r) = \frac{l+1}{2l+1} V_{l,l+\frac{1}{2}}(r) + \frac{l}{2l+1} V_{l,|l-\frac{1}{2}|}(r) \quad (7)$$

and

$$V_l^{\text{SO}}(r) = \frac{2}{2l+1} \left[V_{l,l+\frac{1}{2}}(r) - V_{l,|l-\frac{1}{2}|}(r) \right], \quad (8)$$

respectively. The scalar-relativistic potential, $V_l^{\text{SR}}(r)$, includes the effects of the Darwin term and the mass-velocity term [16]. Hybertsen and Louie [17] considered the effects of the SOC potential, $V_l^{\text{SO}}(r)$, on the spin-orbit splittings in the band structure of semiconductors within first-order perturbation theory, and they found good agreement with experiments.

For computational efficiency, pseudopotentials of the fully separable Kleinman-Bylander (KB) form [18–20] are commonly used instead of those of the semilocal form. The nonlocal part of a fully relativistic KB pseudopotential can be written as

$$\hat{V}_{\text{KB}} = \sum_{l=0}^{l_{\max}} \sum_{j=|l-\frac{1}{2}|}^{l+\frac{1}{2}} \sum_{m_j=-j}^{j} |l, j, m_j\rangle |\beta_{l,j}\rangle \langle \beta_{l,j}| \langle l, j, m_j|, \quad (9)$$

where the radially nonlocal projector $|\beta_{l,j}\rangle\langle\beta_{l,j}|$ is used instead of the radial potential $V_{l,j}(r)$.

Similarly to the case of the semilocal pseudopotential, a fully relativistic KB pseudopotential can be rewritten as the sum of the scalar-relativistic and SOC parts:

$$\hat{V}_{\text{KB}} = \sum_{l=0}^{l_{\max}} |l\rangle \hat{V}_l^{\text{SR}} \langle l| + \sum_{l=1}^{l_{\max}} |l\rangle \hat{V}_l^{\text{SO}} \hat{\mathbf{L}} \cdot \hat{\mathbf{S}} \langle l|, \quad (10)$$

where the nonlocal potentials of the scalar-relativistic and SOC parts of $\hat{V}_{\text{KB}}$ are defined as

$$\hat{V}_l^{\text{SR}} = \frac{l+1}{2l+1} |\beta_{l,l+\frac{1}{2}}\rangle\langle\beta_{l,l+\frac{1}{2}}| + \frac{l}{2l+1} |\beta_{l,|l-\frac{1}{2}|}\rangle\langle\beta_{l,|l-\frac{1}{2}|}| \quad (11)$$

and

$$\hat{V}_l^{\text{SO}} = \frac{2}{2l+1} \left(|\beta_{l,l+\frac{1}{2}}\rangle\langle\beta_{l,l+\frac{1}{2}}| - |\beta_{l,|l-\frac{1}{2}|}\rangle\langle\beta_{l,|l-\frac{1}{2}|}| \right), \quad (12)$$

respectively.

The fully relativistic velocity operator that includes all the nonlocal effects of the fully relativistic KB pseudopotential is written as

$$\hat{\mathbf{v}}^{(\text{FR})} = \hat{\mathbf{v}}^{(\mathbf{p})} + \frac{i}{\hbar} [\hat{V}_{\text{KB}}, \hat{\mathbf{r}}], \quad (13)$$

where $\hat{\mathbf{v}}^{(\mathbf{p})}(= \hat{\mathbf{p}}/m)$ is introduced for notational convenience. The commutator on the right-hand side of Eq. (13) can be separated into scalar-relativistic and SOC parts. By using the expressions in Eqs. (10), (11), and (12), we define the scalar-relativistic velocity operator that includes only the effects arising from the scalar-relativistic part of $\hat{V}_{\text{KB}}$:

$$\hat{\mathbf{v}}^{(\text{SR})} = \hat{\mathbf{v}}^{(\mathbf{p})} + \frac{i}{\hbar} \sum_{l=0}^{l_{\max}} \left[|l\rangle \hat{V}_l^{\text{SR}} \langle l|, \hat{\mathbf{r}} \right]. \quad (14)$$

Within this formalism, the nonlocal effects of SOC on the velocity operator arise from the difference between $\hat{\mathbf{v}}^{(\text{FR})}$ and $\hat{\mathbf{v}}^{(\text{SR})}$, which can be written as the sum of the commutators arising from $\hat{V}_l^{(\text{SO})}$:

$$\hat{\mathbf{v}}^{(\text{SO})} \equiv \hat{\mathbf{v}}^{(\text{FR})} - \hat{\mathbf{v}}^{(\text{SR})} = \sum_{l=1}^{l_{\max}} \hat{\mathbf{v}}_l^{(\text{SO})}, \quad (15)$$

where

$$\hat{\mathbf{v}}_l^{(\text{SO})} = i/\hbar \left[|l\rangle \hat{V}_l^{\text{SO}} \hat{\mathbf{L}} \cdot \hat{\mathbf{S}} \langle l|, \hat{\mathbf{r}} \right]. \quad (16)$$

The optical matrix elements of our interest are $\langle f|\mathbf{e} \cdot \hat{\mathbf{v}}^{(\text{FR/SR/p})}|i\rangle$, where $|i\rangle$ and $|f\rangle$ are the initial and final electronic states, respectively, and $\mathbf{e}$ is the polarization vector of the incident light. We investigate the difference between the matrix elements of $\hat{\mathbf{v}}^{(\text{FR})}$ and $\hat{\mathbf{v}}^{(\text{SR})}$ in several systems having heavy elements such as W and Bi. In the case of an isolated atom, the initial and final states are the eigenstates of angular

momentum operators $|n, l, j, m_j\rangle$, where n is the principal quantum number. In periodic systems, the initial and final states are the Bloch states in the valence band $|v, \mathbf{k}\rangle$ and those in the conduction band $|c, \mathbf{k}\rangle$, respectively, where $\mathbf{k}$ is the crystal momentum, and v and c are the indices of the valence and conduction bands, respectively.

The imaginary part of the dielectric function is calculated within the independent-particle random-phase approximation:

$$\text{Im}\varepsilon^{(\text{P/SR/FR})}(\omega) = \frac{4\pi}{\omega^2 \Omega N_{\mathbf{k}}} \sum_{\mathbf{k}} \sum_{c,v} |\langle c, \mathbf{k}|\mathbf{e} \cdot \hat{\mathbf{v}}^{(\text{P/SR/FR})}|v, \mathbf{k}\rangle|^2$$

$$\times \delta(E_{c,\mathbf{k}} - E_{v,\mathbf{k}} - \hbar\omega), \quad (17)$$

where ω is the frequency of the incident light, Ω is the volume of the unit cell, $N_{\mathbf{k}}$ is the number of $\mathbf{k}$ points in the Brillouin zone, and $E_{v,\mathbf{k}}$ and $E_{c,\mathbf{k}}$ are the Kohn-Sham energy eigenvalues of $|v, \mathbf{k}\rangle$ and $|c, \mathbf{k}\rangle$, respectively.

From Eq. (17), we can see that SOC affects the absorption spectra of materials in two different ways: (i) SOC changes the Kohn-Sham energy eigenvalues, $E_{v,\mathbf{k}}$ and $E_{c,\mathbf{k}}$, and eigenstates, $|c, \mathbf{k}\rangle$ and $|v, \mathbf{k}\rangle$, and (ii) SOC gives an additional contribution, $\hat{\mathbf{v}}^{(\text{SO})}$ in Eq. (15), to the (fully relativistic) velocity operator. The focus of our work is on the second contribution.

In this work, we performed fully relativistic DFT calculations within the generalized gradient approximation [21] using the QUANTUM ESPRESSO package [22,23]. The optical matrix elements and the imaginary part of the dielectric function were calculated by using the YAMBO code [24]. We modified the program so that we can construct both the scalar-relativistic and fully relativistic velocity operators using the same set of fully relativistic KB pseudopotentials. All the fully relativistic KB pseudopotentials used in this work were generated by using the ONCVPSP code [25]. The generating parameters for the pseudopotentials were taken from the work of Schlipf and Gygi [26], while slight modifications were made to get the fully relativistic pseudopotential of Bi.

III. RESULTS AND DISCUSSION

A. Isolated atomic systems

We study the effects of SOC on the optical matrix elements of isolated W and Bi atoms, which are heavy elements and have an electronic structure strongly affected by SOC. We calculated the squared optical matrix elements of the form $|\langle f|\mathbf{e}^+ \cdot \hat{\mathbf{v}}^{(\text{P/SR/FR})}|i\rangle|^2$, where the initial and final states are chosen to be the total angular momentum eigenstates, $|n, l, j, m_j\rangle$, and $\mathbf{e}^+$ is the polarization vector of the left circularly polarized light propagating along the z direction. By comparing the squared matrix elements of $\hat{\mathbf{v}}^{(\text{FR})}$ and $\hat{\mathbf{v}}^{(\text{SR})}$ for a given pair of initial and final states, we calculated the effects of SOC on the individual optical matrix element.

Figures 1(a) and 1(b) show the squared matrix elements of $\hat{\mathbf{v}}^{(\text{FR})}$, $\hat{\mathbf{v}}^{(\text{SR})}$, and $\hat{\mathbf{v}}^{(\text{P})}$. In the case of a W atom, the difference between the squared matrix elements of $\hat{\mathbf{v}}^{(\text{SR})}$ and $\hat{\mathbf{v}}^{(\text{P})}$ is not very large. In the case of a Bi atom, however, the squared matrix elements of $\hat{\mathbf{v}}^{(\text{SR})}$ significantly differ from those of $\hat{\mathbf{v}}^{(\text{P})}$, especially for the $5d \rightarrow 6p$ transitions. It is known that such nonlocal effects arising from the scalar-relativistic part of $\hat{V}_{\text{KB}}$ can be significant if there is a large difference between the l-orbital components of the scalar-relativistic potential, $\hat{V}_l^{\text{SR}}$
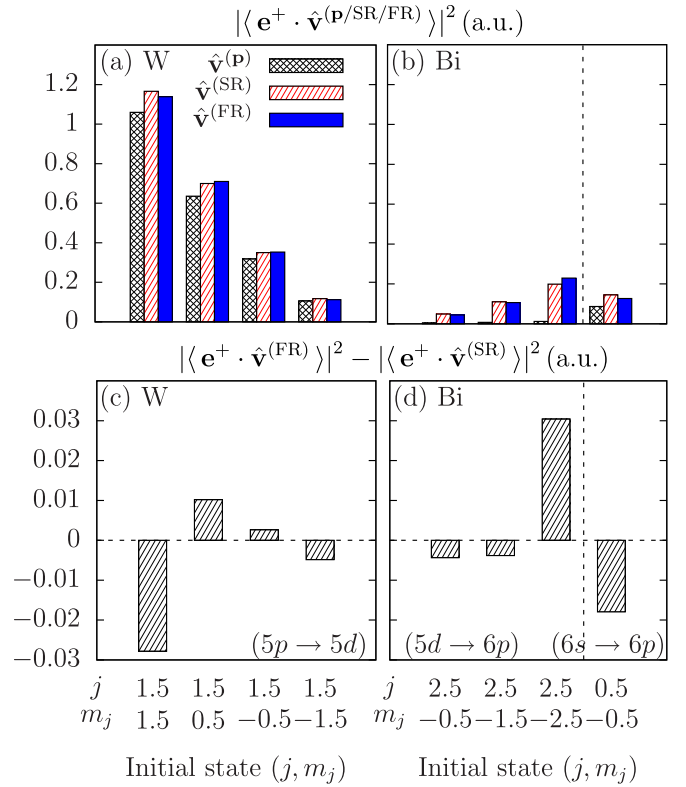

FIG. 1. (a) and (b) The squared optical matrix elements of W and Bi atoms obtained by using the fully relativistic velocity operator, the scalar-relativistic velocity operator, and the momentum operator for the optical transitions between the total angular momentum eigenstates. Only the cases of the largest four squared matrix elements of the fully relativistic velocity operator among $5p \rightarrow 5d$ transitions in a W atom and those among $5d \rightarrow 6p$ and $6s \rightarrow 6p$ transitions in a Bi atom are shown. (c) and (d) The difference between the squared optical matrix elements obtained by using the fully relativistic velocity operator and the scalar-relativistic velocity operator. The incident light is left circularly polarized. The matrix elements are in Hartree.

[24]. On the other hand, the difference between the squared matrix elements of $\hat{\mathbf{v}}^{(\text{FR})}$ and $\hat{\mathbf{v}}^{(\text{SR})}$ is relatively small for all the optical transitions.

Figures 1(c) and 1(d) show the difference between the squared matrix elements of $\hat{\mathbf{v}}^{(\text{FR})}$ and $\hat{\mathbf{v}}^{(\text{SR})}$. In the case of a W atom, the difference between the squared matrix elements of $\hat{\mathbf{v}}^{(\text{FR})}$ and $\hat{\mathbf{v}}^{(\text{SR})}$ can be as large as 4.3% of the squared matrix elements of $\hat{\mathbf{v}}^{(\text{FR})}$. This difference is even more significant for a Bi atom and can reach 14% (in the case of $6s \rightarrow 6p$ transitions). Although the effects of SOC on the optical matrix elements strongly depend upon the characters of the initial and final states, we find that the nonlocal effects of SOC on the optical matrix elements are not negligible in W and Bi atoms.

The relatively large effects of SOC on the optical matrix elements in the case of a Bi atom can be qualitatively understood by looking at the SOC potentials of the W and Bi pseudopotentials in the semilocal form [Eq. (8)]. Figure 2 shows $V_l^{\text{SO}}(r)$ of the W and Bi pseudopotentials used in our calculations (their generating parameters are shown in Table I). Because $V_l^{\text{SO}}(r)$ is defined as the difference between $V_{l,l+1/2}(r)$ and $V_{l,|l-1/2|}(r)$, $V_l^{\text{SO}}(r)$ is localized within the
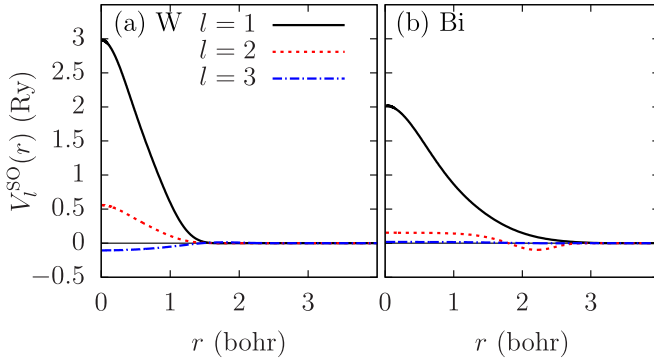
FIG. 2. The spin-orbit coupling potential [Eq. (8)] of the fully relativistic pseudopotentials of W [W(2) pseudopotential in Table I] and Bi atoms.

pseudization radii of $V_{l,l+1/2}(r)$ and $V_{l,|l-1/2|}(r)$. Because the pseudization radii of the W pseudopotential are smaller than those of the Bi pseudopotential (see Table I), $V_l^{SO}(r)$ of the W pseudopotential are more localized than those of the Bi pseudopotential. We note that for both atoms the p-orbital part of the SOC potential, $V_{l=1}^{SO}(r)$, is much larger than the d- and f-orbital parts, $V_{l=2}^{SO}(r)$ and $V_{l=3}^{SO}(r)$.

The matrix elements of $\hat{\mathbf{v}}_l^{(SO)}$ [Eq. (16)] can be explicitly written as

$$\langle f|\hat{\mathbf{v}}_l^{(SO)}|i\rangle = \frac{i}{\hbar}\sum_{\sigma,\sigma'}\int d\mathbf{r}\, V_l^{SO}(r)$$
$$\times \psi_f^*(\mathbf{r},\sigma)[\hat{\mathbf{L}}\cdot\hat{\mathbf{S}}_{\sigma\sigma'}|l\rangle\langle l|l,\mathbf{r}]\psi_i(\mathbf{r},\sigma'), \quad (18)$$

where σ and σ' are the spin indices, and $\psi_i(\mathbf{r},\sigma)$ and $\psi_f(\mathbf{r},\sigma)$ are the $(\mathbf{r},\sigma)$ components of $|i\rangle$ and $|f\rangle$. Because Eq. (18) contains the volume integration of $V_l^{SO}(r)$, not only the value of $V_l^{SO}(r)$ near the core region ($r \sim 0$) but also the spatial extent of $V_l^{SO}(r)$ is an important factor that affects the magnitude of $\langle f|\hat{\mathbf{v}}_l^{(SO)}|i\rangle$.

To sketch the influence of $V_l^{SO}(r)$ on the matrix elements of $\hat{\mathbf{v}}_l^{(SO)}$, we evaluate the volume integration of $|V_l^{SO}(r)|$ for the atoms in the Periodic Table from H ($Z = 1$) to Bi ($Z = 83$) except those in the Lanthanide series (Fig. 3). Roughly speaking, the volume integration of $|V_l^{SO}(r)|$ increases with the atomic number Z, or with the atomic mass. For example, the volume integration of $|V_{l=1}^{SO}(r)|$ of the Bi ($Z = 83$) pseudopotential is 0.78 Hartree, while the same quantity of the W ($Z = 74$) pseudopotential is 0.3. The result is consistent with

our observation in Fig. 1 that the effects of SOC on the optical matrix elements increase with the atomic mass (4.3% and 14% of the squared matrix elements of $\hat{\mathbf{v}}^{(FR)}$ for W and Bi atoms, respectively).

For most atoms in Fig. 3, we find that the p-orbital component of the SOC potential, $|V_{l=1}^{SO}(r)|$, is the largest; the d-orbital component, $|V_{l=2}^{SO}(r)|$, is the second largest; and the f-orbital component, $|V_{l=3}^{SO}(r)|$, is the smallest. Therefore, it is natural to expect that the contribution of $\hat{\mathbf{v}}_{l=1}^{(SO)}$ to the optical matrix elements is the most important one and that the contribution of $\hat{\mathbf{v}}_l^{(SO)}$ becomes smaller as l increases. To investigate the contribution of $\hat{\mathbf{v}}_l^{(SO)}$ to the squared matrix elements of $\hat{\mathbf{v}}^{(FR)}$, we calculated the squared matrix elements of $\hat{\mathbf{v}}^{(FR)}$ and $\hat{\mathbf{v}}^{(FR)} - \hat{\mathbf{v}}_l^{(SO)}$.

Figure 4 shows the difference between the squared matrix elements of $\hat{\mathbf{v}}^{(FR)}$ and $\hat{\mathbf{v}}^{(FR)} - \hat{\mathbf{v}}_l^{(SO)}$ in the cases of W and Bi atoms. In both cases, the contribution of $\hat{\mathbf{v}}_{l=1}^{(SO)}$ to the squared matrix elements of $\hat{\mathbf{v}}^{(FR)}$ is the largest among the contributions of $\hat{\mathbf{v}}_l^{(SO)}$. The contribution of $\hat{\mathbf{v}}_{l=2}^{(SO)}$ is the second largest and that of $\hat{\mathbf{v}}_{l=3}^{(SO)}$ is the smallest and negligible. In the case of a W atom, there is a case in which the contribution of $\hat{\mathbf{v}}_{l=2}^{(SO)}$ is almost half of the contribution of $\hat{\mathbf{v}}_{l=1}^{(SO)}$. In the case of a Bi atom, the contributions of $\hat{\mathbf{v}}_{l=2}^{(SO)}$ and $\hat{\mathbf{v}}_{l=3}^{(SO)}$ are very small.

Because $\hat{\mathbf{v}}_l^{(SO)}$ contains the orbital angular momentum projector, $|l\rangle\langle l|$, the matrix elements of $\hat{\mathbf{v}}_l^{(SO)}$ are finite only if the initial state or the final state has l-orbital angular momentum character. In addition, according to the optical selection rule, the matrix elements $\langle f|\hat{\mathbf{v}}_l^{(SO)}|i\rangle$ are finite if the difference between the l's of $|i\rangle$ and $|f\rangle$ is ± 1. Therefore, the matrix elements of $\hat{\mathbf{v}}_{l=3}^{(SO)}$ are finite only for the transitions between the states that have d- and f-orbital angular momentum characters. In our calculations, the contribution of $\hat{\mathbf{v}}_{l=3}^{(SO)}$ to the squared matrix elements of $\hat{\mathbf{v}}^{(FR)}$ is usually very small for such transitions.

It is known that the effects of SOC on the energy levels and wave functions of atomic systems are the largest for p-orbitals and become smaller for d- and f-orbitals [27]. In fact, if we recall the fine structure of a hydrogen atom, we easily see that the energy splittings induced by SOC show the same l-dependent behavior ($p > d > f$) [28].[1] Our results are in line with these relativistic effects on atomic systems.

B. Monolayer transition-metal dichalcogenides

We calculate the optical matrix elements and absorption spectra of a monolayer of four 2H-type semiconducting TMDCs (MoS_2, $MoSe_2$, WS_2, and WSe_2). Figure 5(a) shows the structure of the two-dimensional crystal. The TMDC monolayer of 2H-type consists of a transition-metal layer (Mo or W) that is sandwiched by two chalcogen layers (S or Se). Figure 5(b) shows the two-dimensional Brillouin zone.

In our DFT calculations using fully relativistic pseudopotentials, we set the kinetic energy cutoff of the plane-wave basis to 80 Ry and sample the Brillouin zone with a $12 \times 12 \times 1$

TABLE I. Pseudopotentials used in this work. The pseudization radii of the pseudo-wave-functions with different orbital angular momenta, r_s, r_p, r_d, and r_f, are shown in units of the Bohr radius.

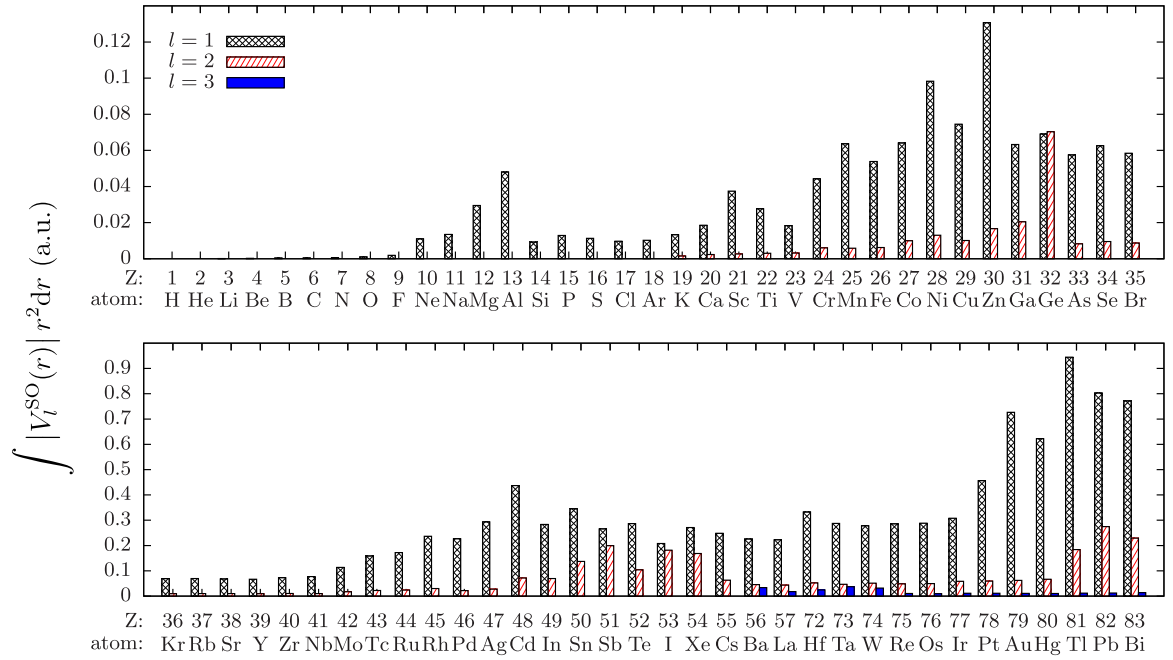|	Core	Valence	r_s	r_p	r_d	r_f
S	[Ne]	$3s^2 3p^4$	2.12	1.51		
Se	[Ar] $3d^{10}$	$4s^2 4p^4$	2.60	2.71	3.33	
Mo	[Ar] $3d^{10}$	$4s^2 4p^6 5s^2 4d^4$	2.00	2.50	2.56	
W(1)	[Kr] $4d^{10}$	$4f^{14} 5s^2 5p^6 6s^2 5d^4$	2.12	2.19	1.88	3.03
W(2)	[Kr] $4d^{10} 4f^{14}$	$5s^2 5p^6 6s^2 5d^4$	2.02	1.93	1.84	2.73
Bi	[Xe] $4f^{14}$	$5d^{10} 6s^2 6p^3$	3.19	3.15	3.00	3.34

—————

[1]See, for example, Fig. 6.9 of Ref. [28].

FIG. 3. The volume integration of $|V_l^{\text{SO}}(r)|$ [see Eq. (8)] of the fully relativistic pseudopotentials of the atoms from H ($Z = 1$) to Bi ($Z = 83$) except those in the Lanthanide series.

Monkhorst-Pack grid [29]. In calculations of absorption spectra, we use a denser $120 \times 120 \times 1$ Monkhorst-Pack grid for **k**-point summations.

Figures 5(c)–5(f) show the electronic band structure of TMDC monolayers. At the valence-band maximum at K, we see energy splittings between the two highest bands in the valence thanks to the large SOC of $4d$ and $5d$ transition metals. The magnitude of the SOC-induced energy splittings varies from 153 to 468 meV (larger for the TMDCs having W atoms). All the results of our calculations are consistent with previous theoretical studies [30,31].

To investigate the effects of SOC on the absorption spectra of monolayer TMDCs, we calculated the imaginary part of the independent-particle dielectric function using $\hat{\mathbf{v}}^{(\text{FR})}$, $\hat{\mathbf{v}}^{(\text{SR})}$, and

$\hat{\mathbf{v}}^{(\mathbf{p})}$: $\text{Im}\,\varepsilon^{(\text{FR})}(\omega)$, $\text{Im}\,\varepsilon^{(\text{SR})}(\omega)$, and $\text{Im}\,\varepsilon^{(\mathbf{p})}(\omega)$. Figures 6(a)–6(d) show $\text{Im}\,\varepsilon^{(\text{FR})}(\omega)$ of monolayer TMDCs. The onset energies of $\text{Im}\,\varepsilon^{(\text{FR})}(\omega)$ correspond to the band gaps of monolayer TMDCs. In the low-energy regime ($\hbar\omega < 2$ eV), we see step-function-like behaviors of $\text{Im}\,\varepsilon^{(\text{FR})}(\omega)$, which mainly result from the optical transitions between the band-edge states at K and K', i.e., the two highest-energy valence and the two lowest-energy conduction bands. These band-edge states mostly consist of the d orbitals of transition-metal atoms and the p orbitals of chalcogen atoms. In the high-energy regime
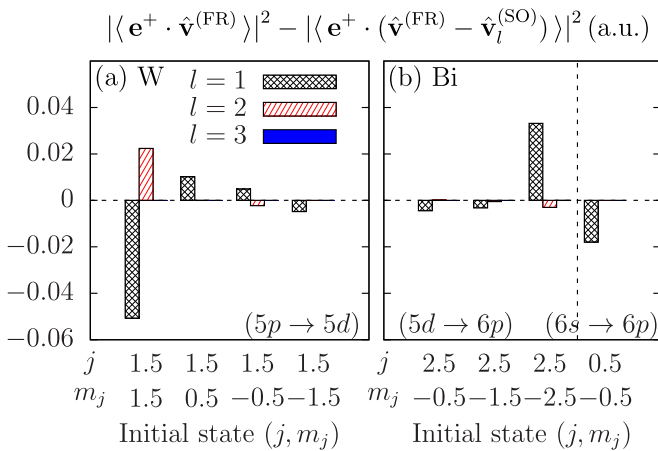

FIG. 4. The difference between the squared matrix elements of W and Bi atoms obtained by using the fully relativistic velocity operator and $\hat{\mathbf{v}}^{(\text{FR})} - \hat{\mathbf{v}}_l^{(\text{SO})}$ [see Eqs. (13) and (16)]. The initial and final states are the same as those in Fig. 1.
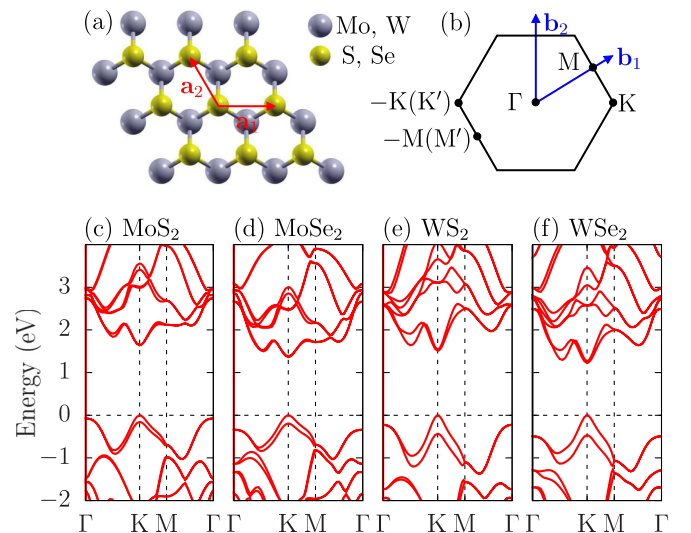
FIG. 5. (a) and (b) The crystal structure and the Brillouin zone of a monolayer of 2H-type semiconducting transition-metal dichalcogenides, respectively. (c)–(f) The electronic band structure of a monolayer of four 2H-type transition-metal dichalcogenides.
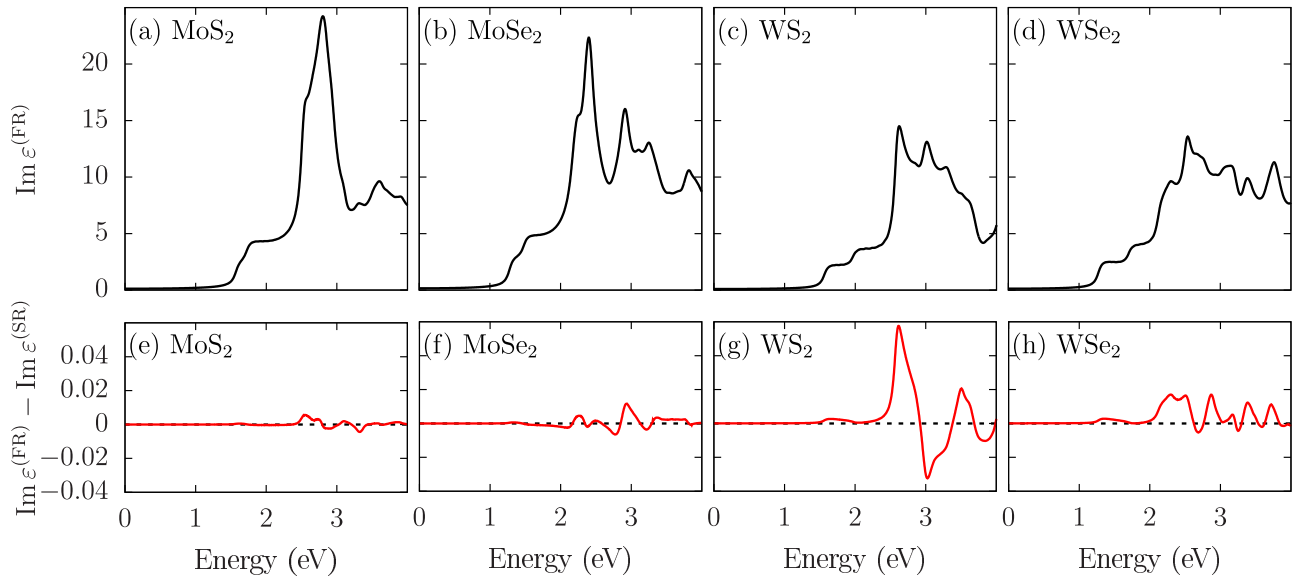
FIG. 6. (a)–(d) The imaginary part of the dielectric function of monolayer transition-metal dichalcogenides obtained by using the fully relativistic velocity operator. (e)–(h) The difference between the imaginary part of the dielectric functions of monolayer transition-metal dichalcogenides obtained by using the fully relativistic velocity operator and the scalar-relativistic velocity operator.

($\hbar\omega > 2$ eV), additional sharp features arise as the states other than the band-edge states make contributions to Im $\varepsilon^{(\mathrm{FR})}(\omega)$.

Figures 6(e)–6(h) show the difference between Im $\varepsilon^{(\mathrm{FR})}(\omega)$ and Im $\varepsilon^{(\mathrm{SR})}(\omega)$. In the low-energy regime ($\hbar\omega < 2$ eV), the difference between Im $\varepsilon^{(\mathrm{FR})}(\omega)$ and Im $\varepsilon^{(\mathrm{SR})}(\omega)$ is three orders of magnitude smaller than Im $\varepsilon^{(\mathrm{FR})}(\omega)$ itself, which indicates that the nonlocal effects of SOC on Im $\varepsilon^{(\mathrm{FR})}(\omega)$ are negligibly small in this range of energy. The effects of SOC become larger at higher energies ($\hbar\omega > 2$ eV). This is because the initial states with lower band energies start to be involved. They largely consist of p-orbitals ($4p$ for Mo and $5p$ for W), which are very localized near the core of transition-metal atoms. These lower band energy states are responsible for the increase of the effects of spin-orbit coupling on Im $\varepsilon^{(\mathrm{FR})}(\omega)$ at higher energies. However, the difference between Im $\varepsilon^{(\mathrm{FR})}(\omega)$ and Im $\varepsilon^{(\mathrm{SR})}(\omega)$ remains smaller than 1% of Im $\varepsilon^{(\mathrm{FR})}(\omega)$.

In general, the nonlocal part of a pseudopotential strongly depends on its generating parameters, such as valence (and core) configurations, pseudization radii, and the local part of the pseudopotential. Therefore, the effects of the commutator on the optical matrix elements and absorption spectra of a material (including the contributions from the scalar-relativistic and SOC parts of the pseudopotential) can change significantly by the nonlocal character of the pseudopotential used in the calculations.

In Fig. 7, we plot the imaginary part of the dielectric function of monolayer WSe$_2$ obtained by using two different fully relativistic KB pseudopotentials of W (for comparison, we fixed the pseudopotential of Se). We checked that the two different pseudopotentials of W yield almost the same band structure within the energy range of our interest ($\hbar\omega = 0$–4 eV). The absorption spectra in Figs. 7(a) and 7(c) were obtained by using a W pseudopotential that includes $4f$ electrons in the valence [see W(1) in Table I], while those in Figs. 7(b) and 7(d) were obtained by using a W pseudopotential that includes $4f$ electrons in the core [see W(2) in Table I].

By comparing Im $\varepsilon^{(\mathbf{p})}(\omega)$ in Figs. 7(a) and 7(b), we find that the absorption spectrum strongly depends on the pseudopotential of W if we neglect all the effects arising from the nonlocal part of the pseudopotential and use $\hat{\mathbf{v}}^{(\mathbf{p})}$ as the velocity operator. In the case of the W(1) pseudopotential,
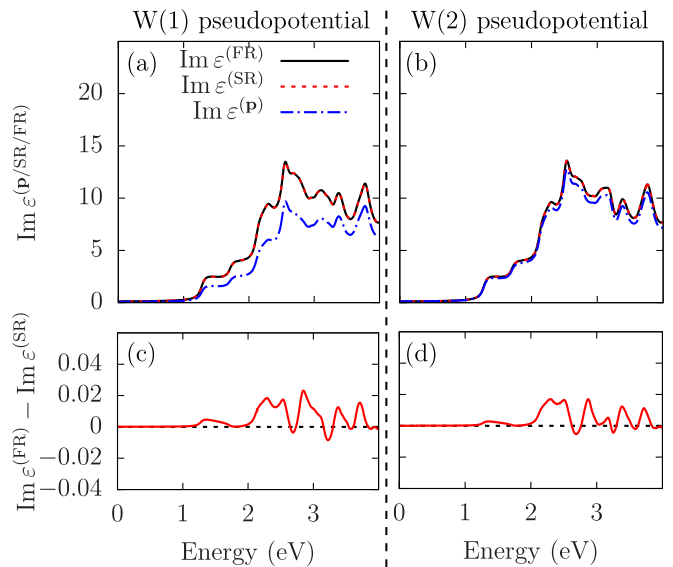

FIG. 7. (a) and (b) The imaginary part of the dielectric function of monolayer WSe$_2$ obtained by using two different pseudopotentials of W, which were generated from two different valence configurations (see Table I for details). Im $\varepsilon^{(\mathbf{p})}(\omega)$, Im $\varepsilon^{(\mathrm{SR})}(\omega)$, and Im $\varepsilon^{(\mathrm{FR})}(\omega)$ are the imaginary part of the dielectric function obtained by using the momentum operator, the scalar-relativistic velocity operator, and the fully relativistic velocity operator, respectively. (c) and (d) The difference between the imaginary part of the dielectric function obtained by using the fully relativistic and the scalar-relativistic velocity operators.
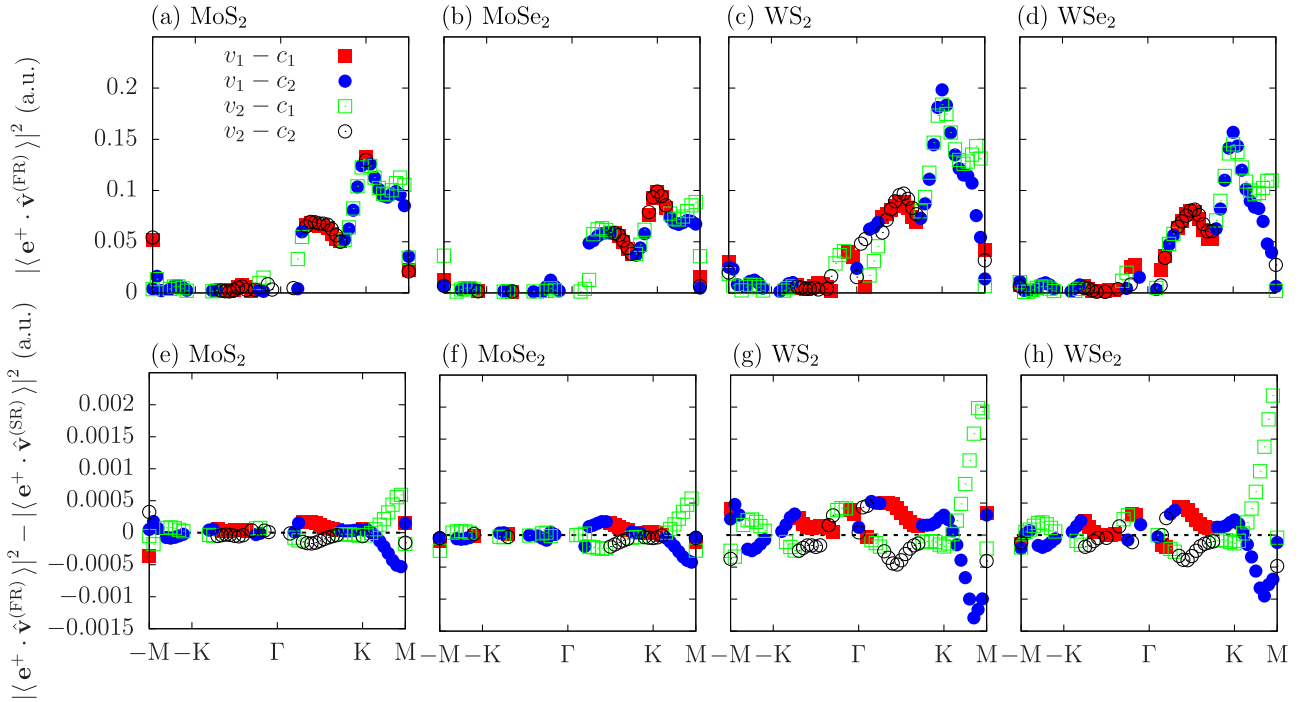
FIG. 8. (a)–(d) The squared optical matrix elements obtained by using the fully relativistic velocity operator of monolayer transition-metal dichalcogenides for the optical transitions involving the highest-energy and second-highest-energy states in the valence band, v_1 and v_2, respectively, and the lowest-energy and second-lowest-energy states in the conduction band, c_1 and c_2, respectively. The squared optical matrix elements were calculated along the path in the momentum space, $-M \rightarrow -K \rightarrow \Gamma \rightarrow K \rightarrow M$. (e)–(h) The difference between the squared optical matrix elements obtained by using the fully relativistic velocity operator and those obtained by using the scalar-relativistic velocity operator. In all cases, the incident light is left circularly polarized.

Im $\varepsilon^{(\mathbf{p})}(\omega)$ is much smaller than Im $\varepsilon^{(\mathrm{SR})}(\omega)$. The result shows that the commutator arising from the scalar-relativistic part of the W(1) pseudopotential affects strongly the absorption spectrum. The large difference between Im $\varepsilon^{(\mathrm{SR})}(\omega)$ and Im $\varepsilon^{(\mathbf{p})}(\omega)$ is attributed to the presence of $4f$ electrons in the valence, which makes the W(1) pseudopotential strongly nonlocal. On the other hand, in the case of the W(2) pseudopotential, Im $\varepsilon^{(\mathbf{p})}(\omega)$ is quite similar to Im $\varepsilon^{(\mathrm{SR})}(\omega)$. The effects of the commutator arising from the scalar-relativistic part of the pseudopotential are much smaller for the W(2) pseudopotential where $4f$ electrons are treated as core electrons. We note that in both cases, Im $\varepsilon^{(\mathrm{SR})}(\omega)$ is almost identical to Im $\varepsilon^{(\mathrm{FR})}(\omega)$.

Figures 7(c) and 7(d) show the difference between Im $\varepsilon^{(\mathrm{FR})}(\omega)$ and Im $\varepsilon^{(\mathrm{SR})}(\omega)$. We find that the contributions of SOC to Im $\varepsilon^{(\mathrm{FR})}(\omega)$ for the two different pseudopotentials of W are very similar to each other in the whole energy range. The result shows that the effects of the commutator arising from SOC on the absorption spectra do not depend much on the pseudopotential.

It is possible that even if the nonlocal effects of SOC on the individual optical matrix element are large, the effects on the absorption spectrum are small as we sum over the contributions from many optical matrix elements with different momenta and band indices. To check this possibility, we calculated the squared matrix elements $|\langle c_i, \mathbf{k} | \mathbf{e}^+ \cdot \hat{\mathbf{v}}^{(\mathrm{SR/FR})} | v_j, \mathbf{k} \rangle|^2$, where i and j are 1 or 2, v_1 and v_2 are the band indices of the highest-energy and second-highest-energy states in the valence band, respectively, c_1 and c_2 are the band

indices of the lowest-energy and second-lowest-energy states in the conduction band, respectively, and $\mathbf{k}$ is on the path $-M \rightarrow -K \rightarrow \Gamma \rightarrow K \rightarrow M$ [Fig. 5(b)].

Figures 8(a)–8(d) show the squared matrix elements of $\hat{\mathbf{v}}^{(\mathrm{FR})}$. Here, we see that the squared matrix elements of $\hat{\mathbf{v}}^{(\mathrm{FR})}$ near K are larger in magnitude than those near $-K$. Because we assumed the incident light to be left circularly polarized, the result can be explained by the valley-selective circular dichroism of monolayer TMDCs [32].

Figures 8(e)–8(h) show the difference between the squared matrix elements of $\hat{\mathbf{v}}^{(\mathrm{FR})}$ and $\hat{\mathbf{v}}^{(\mathrm{SR})}$. Although the contribution of the commutator arising from SOC to the squared matrix elements of $\hat{\mathbf{v}}^{(\mathrm{FR})}$ becomes larger in the case of having heavier transition-metal atoms (WS$_2$ and WSe$_2$), even in those cases the contribution from SOC remains smaller than 1% of the squared matrix elements of $\hat{\mathbf{v}}^{(\mathrm{FR})}$. If we compare this result with the previous result of an isolated W atom, the influence of the commutator arising from SOC on the optical matrix elements is much suppressed: In the case of a W atom, the effects of SOC on the squared optical matrix elements can be as large as 4.3% of the squared matrix elements of $\hat{\mathbf{v}}^{(\mathrm{FR})}$ [Figs. 1(a) and 1(c)].

Next, we further investigate the dependence of the squared matrix elements of $\hat{\mathbf{v}}^{(\mathrm{FR})}$, $\hat{\mathbf{v}}^{(\mathrm{SR})}$, and $\hat{\mathbf{v}}^{(\mathbf{p})}$ on the initial and final states in the case of monolayer WSe$_2$. We calculated the squared matrix elements at K, $|\langle c, K | \mathbf{e}^+ \cdot \hat{\mathbf{v}}^{(\mathbf{p}/\mathrm{SR/FR})} | v, K \rangle|^2$, where v and c are the band indices of the initial and final states, respectively. The band indices are in increasing order of energy (the state at the valence-band maximum is $v = 26$). We
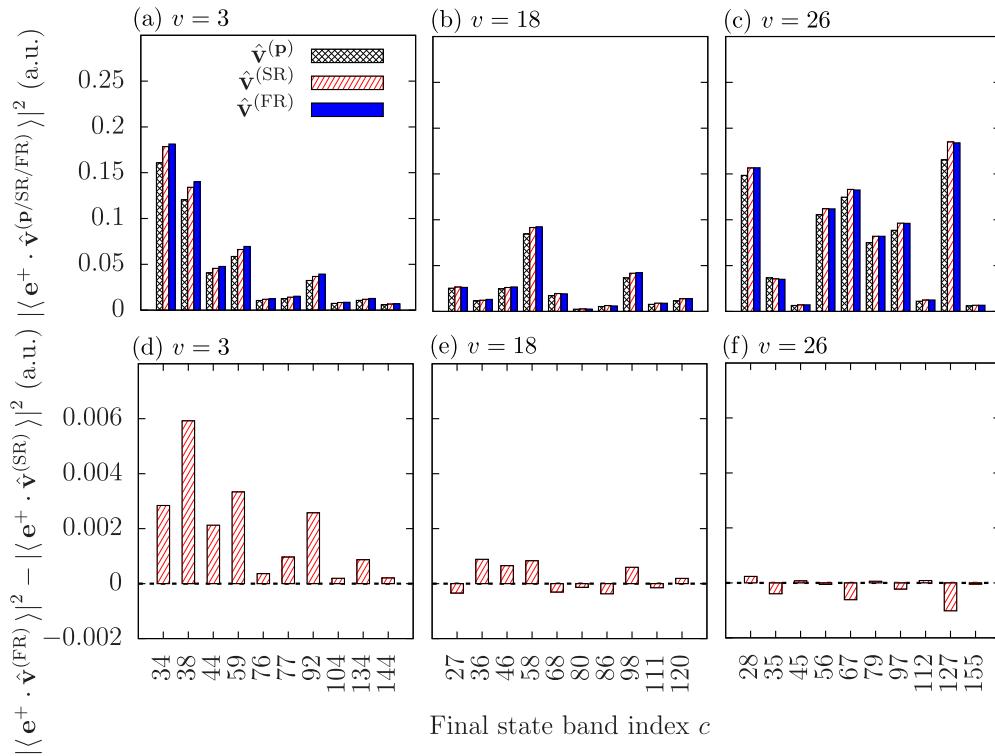
FIG. 9. (a)–(c) The squared optical matrix elements of monolayer WSe_2 obtained by using the fully relativistic velocity operator, the scalar-relativistic operator, and the momentum operator for the optical transitions at K in the momentum space. (d)–(f) The difference between the squared optical matrix elements obtained by using the fully relativistic velocity operator and the scalar-relativistic operator. In all cases, left circularly polarized light was considered.

consider three initial states having different orbital characters: (i) $|3, K\rangle$, which mostly consists of the $5p$ orbitals of W atoms, (ii) $|18, K\rangle$, which consists of the $5p$ and $4d$ orbitals of W atoms and the $3p$ orbitals of Se atoms, and (iii) $|26, K\rangle$, which consists of the $4d$ orbitals of W atoms and the $3p$ orbitals of Se atoms. For each initial state, we consider all the final states satisfying $E_{c,K} - E_{v,K} < 1$ Ry.

Figures 9(a)–9(c) show the squared matrix elements of $\hat{v}^{(FR)}$, $\hat{v}^{(SR)}$, and $\hat{v}^{(p)}$ and Figs. 9(d)–9(f) show the difference between the squared matrix elements of $\hat{v}^{(FR)}$ and $\hat{v}^{(SR)}$. By comparing the results of Figs. 9(d), 9(e), and 9(f), we find that the effects of SOC on the optical matrix elements are larger for the optical transitions whose initial state is more localized at W atoms. In the case of $|3, K\rangle$, the effects of SOC on the squared matrix elements of $\hat{v}^{(FR)}$ can be as large as 6.8%, while in the case of $|26, K\rangle$, the effects are much smaller, less than 1.1%. The result of $|18, K\rangle$ falls somewhere between the results of $|3, K\rangle$ and $|26, K\rangle$.

Figure 10 show the differences between the squared matrix elements of $\hat{v}^{(FR)}$ and $\hat{v}^{(FR)} - \hat{v}_l^{(SO)}$ for the optical transitions having $|3, K\rangle$, $|18, K\rangle$, and $|26, K\rangle$ as the initial states. In the case of $|3, K\rangle$, we find that among $\hat{v}_l^{(SO)}$'s, $\hat{v}_{l=1}^{(SO)}$ gives the largest contribution to the squared matrix elements of $\hat{v}^{(FR)}$. The d-orbital part $\hat{v}_{l=2}^{(SO)}$ gives the second largest contribution and the contribution from the f-orbital part $\hat{v}_{l=3}^{(SO)}$ is negligible. This result is similar to the result of an isolated W atom [Fig. 4(a)].

Figures 10(b) and 10(c) show that $\hat{v}_{l=1}^{(SO)}$ is relatively less important in the cases of $|18, K\rangle$ and $|26, K\rangle$ than in the

case of $|3, K\rangle$. The result can be qualitatively understood by looking at the W p- and d-orbital characters of the initial states. As we move from $|3, K\rangle$ to $|18, K\rangle$ and $|26, K\rangle$, the proportion of the W $5p$-orbital component in the initial state decreases while that of the W $4d$-orbital component increases. In the case of $|26, K\rangle$, because the initial state mostly consists of the W $4d$ orbitals, the matrix elements of $\hat{v}_{l=1}^{(SO)}$ are finite only for the final states having W $6p$-orbital character ($\Delta l = \pm 1$). Such final states are much more delocalized than the initial state, and the matrix elements of $\hat{v}_{l=1}^{(SO)}$ are small.

C. Bi_2Se_3 and Bi_2Te_3

We investigate the effects of SOC on the optical matrix elements of five-quintuple-layer slabs of Bi_2Se_3 and Bi_2Te_3. Here, we focus on the optical transitions whose initial states are the topological surface states. In DFT calculations, we slightly broke the inversion symmetry to induce small energy splittings between the surface states localized at the top and bottom sides of Bi_2Se_3 and Bi_2Te_3 slabs. In this way, we can obtain the surface states $|v, \mathbf{k}\rangle$ (v is the band index and $v = 241$ and 391 for Bi_2Se_3 and Bi_2Te_3, respectively), which are localized well on each surface of the slabs. In the calculation of the optical matrix elements, we chose the surface state with momentum $\mathbf{k} = 0.05$ ΓK as our initial state [blue dots in Figs. 11(a) and 11(b)]. Also here, we consider all the final states that satisfy $E_{c,\mathbf{k}} - E_{v,\mathbf{k}} < 1$ Ry. We set the kinetic energy cutoff of the plane-wave basis to 80 Ry and use a $6 \times 6 \times 1$ Monkhorst-Pack grid for $\mathbf{k}$-point sampling.
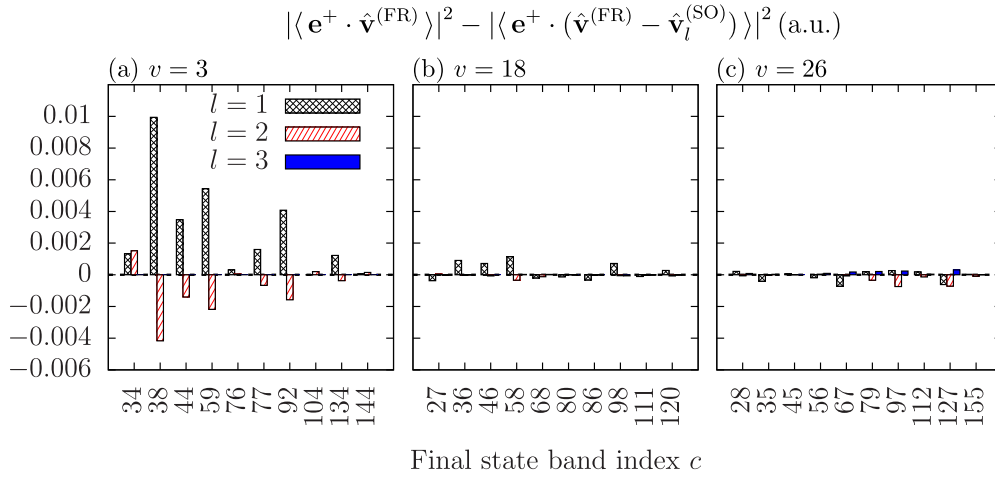
$$|\langle \mathbf{e}^{+} \cdot \hat{\mathbf{v}}^{(\mathrm{FR})} \rangle|^{2} - |\langle \mathbf{e}^{+} \cdot (\hat{\mathbf{v}}^{(\mathrm{FR})} - \hat{\mathbf{v}}_{l}^{(\mathrm{SO})}) \rangle|^{2} \; (\mathrm{a.u.})$$

FIG. 10. (a)–(c) The difference between the squared matrix elements of monolayer WSe_2 obtained by using the fully relativistic velocity operator and $\hat{\mathbf{v}}^{(\mathrm{FR})} - \hat{\mathbf{v}}_{l}^{(\mathrm{SO})}$ [see Eqs. (13) and (15)] for the optical transitions at K in the momentum space. In all cases, left circularly polarized light was considered.

Figures 12(a) and 12(b) show the squared matrix elements of $\hat{\mathbf{v}}^{(\mathrm{FR})}$, $\hat{\mathbf{v}}^{(\mathrm{SR})}$, and $\hat{\mathbf{v}}^{(\mathbf{p})}$. We find that the difference between the squared matrix elements of $\hat{\mathbf{v}}^{(\mathrm{FR})}$ and $\hat{\mathbf{v}}^{(\mathrm{SR})}$ is very small, while the difference between the squared matrix elements of $\hat{\mathbf{v}}^{(\mathrm{SR})}$ and $\hat{\mathbf{v}}^{(\mathbf{p})}$ is large in some cases of Bi_2Te_3. Figures 12(c) and 12(d) show the differences between the squared matrix elements of $\hat{\mathbf{v}}^{(\mathrm{FR})}$ and $\hat{\mathbf{v}}^{(\mathrm{SR})}$ in a different scale. As in the case of the transitions from the valence-band maximum of monolayer WSe_2 [Figs. 9(c) and 9(f)], the effects of SOC on the optical matrix elements of Bi_2Se_3 and Bi_2Te_3 slabs are very small (less than 1% of the squared matrix elements of $\hat{\mathbf{v}}^{(\mathrm{FR})}$).

Figure 13 shows the difference between the squared matrix elements of $\hat{\mathbf{v}}^{(\mathrm{FR})}$ and $\hat{\mathbf{v}}^{(\mathrm{FR})} - \hat{\mathbf{v}}_{l}^{(\mathrm{SO})}$ for the same optical transitions presented in Fig. 12. We find that the effects of the p-orbital part $\hat{\mathbf{v}}_{l=1}^{(\mathrm{SO})}$ on the optical matrix elements are usually the largest, and the effects of the d- and f-orbital parts, $\hat{\mathbf{v}}_{l=2}^{(\mathrm{SO})}$ and $\hat{\mathbf{v}}_{l=3}^{(\mathrm{SO})}$, are much smaller. This is because (i) the p-orbital component of the SOC potential $V_{l=1}^{\mathrm{SO}}(r)$ of Bi is much larger than the d- and f-orbital components $V_{l=2,3}^{\mathrm{SO}}(r)$ (see Figs. 2 and 3), and (ii) in particular, the surface states of Bi_2Se_3 and Bi_2Te_3 mostly consist of the $6p$ orbitals of Bi atoms.

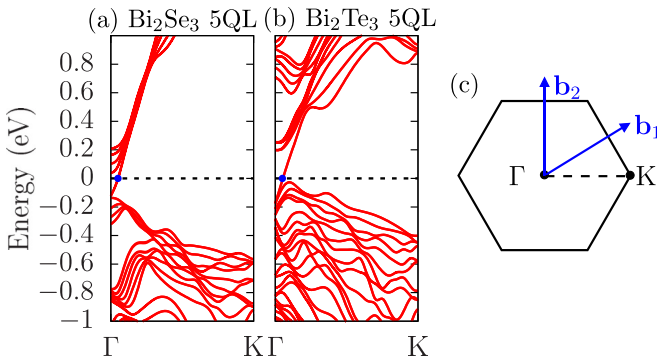The circular dichroism is defined as the relative difference between the squared optical matrix elements for left- and right-circularly-polarized light (see the top of Fig. 14). We calculated the circular dichroism by using $\hat{\mathbf{v}}^{(\mathrm{FR})}$ and $\hat{\mathbf{v}}^{(\mathrm{SR})}$ and
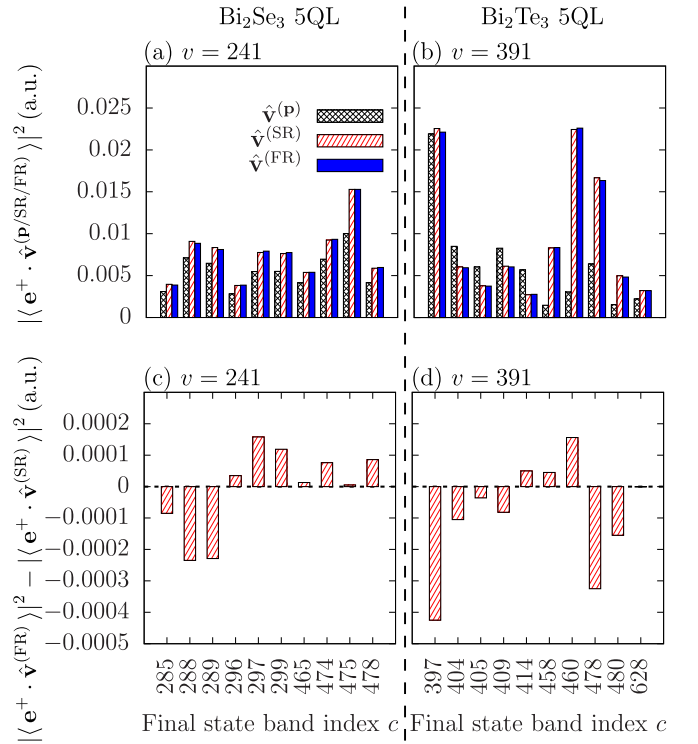

FIG. 12. (a) and (b) The squared optical matrix elements of five-quintuple-layer slabs of Bi_2Se_3 and Bi_2Te_3 obtained by using the fully relativistic velocity operator, the scalar-relativistic operator, and the momentum operator for the optical transitions having the topological surface state with momentum $\mathbf{k} = 0.05\,\Gamma K$ as the initial state. (c) and (d) The difference between the squared optical matrix elements obtained by using the fully relativistic velocity operator and the scalar-relativistic operator. In all cases, left circularly polarized light was considered.
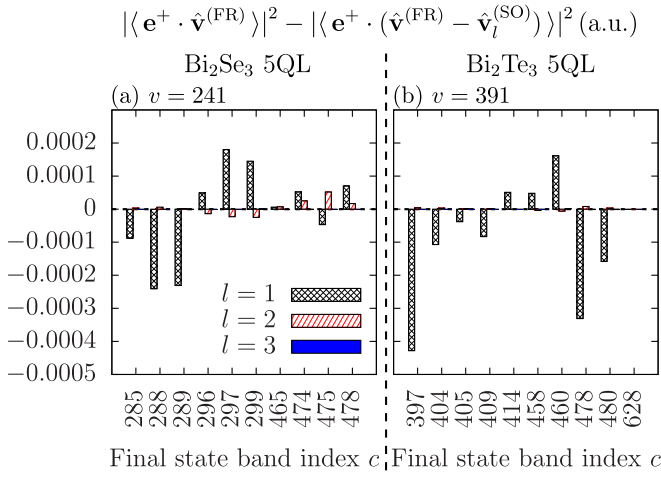

FIG. 11. (a) and (b) The electronic band structure of five-quintuple-layer slabs of Bi_2Se_3 and Bi_2Te_3. (c) The Brillouin zone of five-quintuple-layer slabs of Bi_2Se_3 and Bi_2Te_3.

FIG. 13. The difference between the squared matrix elements of five-quintuple-layer slabs of Bi_2Se_3 and Bi_2Te_3 obtained by using the fully relativistic velocity operator and $\hat{\mathbf{v}}^{(FR)} - \hat{\mathbf{v}}_l^{(SO)}$ [see Eqs. (13) and (15)] for the optical transitions having the topological surface state with momentum $\mathbf{k} = 0.05\,\Gamma K$ as the initial state. In all cases, left circularly polarized light was considered.

investigated whether the effects of the commutator arising from SOC change the circular dichroism of Bi_2Se_3 and Bi_2Te_3 slabs.

In Fig. 14, we see that the difference between the circular dichroisms obtained by using $\hat{\mathbf{v}}^{(FR)}$ and $\hat{\mathbf{v}}^{(SR)}$ is negligible. Contrary to the arguments in Ref. [12], the effects of the commutator arising from SOC cannot change the circular dichroism of Bi_2Se_3 and Bi_2Te_3 slabs, which means that the methods used in Refs. [5,6,11] will give correct results. Although we did not find the correct final states (satisfying the proper boundary condition) in the calculations of the optical matrix elements, because the effects of SOC on the optical matrix elements are negligible over a wide range of
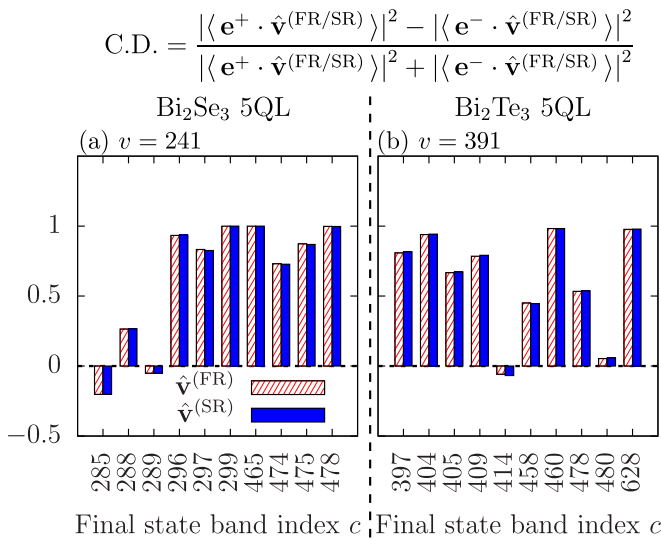

FIG. 14. The circular dichroism of five-quintuple-layer slabs of Bi_2Se_3 and Bi_2Te_3 for the optical transitions having the topological surface state with momentum $\mathbf{k} = 0.05\,\Gamma K$ as the initial state.

energies ($E_{c,\mathbf{k}} - E_{v,\mathbf{k}} < 1$ Ry), it is likely that imposing the correct boundary condition on the final states will not make a significant difference between the results obtained by using $\hat{\mathbf{v}}^{(FR)}$ and $\hat{\mathbf{v}}^{(SR)}$.

IV. CONCLUSION

In this study, we investigated the effects of spin-orbit coupling on the optical responses of isolated atoms, monolayer transition-metal dichalcogenides, and the topological surface states of topological insulators using first-principles calculations with fully relativistic pseudopotentials. By using a method that can separate a fully relativistic Kleinman-Bylander pseudopotential into the scalar-relativistic and spin-orbit coupling parts, we were able to study the effects of spin-orbit coupling on the velocity operator and its matrix elements in various systems.

In the case of W and Bi atoms, we find that the relative contribution of the commutator arising from spin-orbit coupling to the squared optical matrix elements can be 4.3% for W and 14% for Bi. We find that the p-orbital part of the commutator arising from spin-orbit coupling gives the largest contribution to the optical matrix elements. The influence of the p-orbital part of the spin-orbit coupling potential is much larger than those of the d- and f-orbital parts.

In the case of monolayer transition-metal dichalcogenides, the effects of the commutator arising from spin-orbit coupling are much smaller than in the case of atomic systems, less than 1% of the squared optical matrix elements for the optical transitions from the valence-band edge states.

In the case of five-quintuple layer slabs of Bi_2Se_3 and Bi_2Te_3, the effects of spin-orbit coupling on the optical matrix elements are again very small as in the case of monolayer transition-metal dichalcogenides. We find that the nonlocal effects of spin-orbit coupling on the optical matrix elements are so small that the effects do not change the circular dichroism of Bi_2Se_3 and Bi_2Te_3 slabs.

In conclusion, we confirm that while the effects of the commutator arising from spin-orbit coupling on the optical matrix elements are not negligible in atomic systems, the effects are much suppressed in the cases of monolayer transition-metal dichalcogenides and topological insulators where the effects of spin-orbit coupling on the electronic structure are considered to be important.

Although all of our calculations were done within DFT, we expect that the general conclusion will be similar even if we consider many-body approaches in our calculations. Within the GW approximation, many-body effects on the optical matrix elements can be accounted for by correcting the matrix elements: the renormalization of the optical matrix elements, $\langle c, \mathbf{k} | \hat{\mathbf{v}} | v, \mathbf{k} \rangle^{LDA}$, that were obtained from the calculations using the local density approximation (LDA) is given as $\langle c, \mathbf{k} | \hat{\mathbf{v}} | v, \mathbf{k} \rangle^{LDA} \times (E_{c,\mathbf{k}}^{GW} - E_{v,\mathbf{k}}^{GW})/(E_{c,\mathbf{k}}^{LDA} - E_{v,\mathbf{k}}^{LDA})$ [33,34], where $\mathbf{k}$ is the crystal momentum, $|c, \mathbf{k}\rangle$ and $|v, \mathbf{k}\rangle$ are the LDA wave functions of the conduction and valence bands, respectively, and $E_{c,\mathbf{k}}^{GW} - E_{v,\mathbf{k}}^{GW}$ and $E_{c,\mathbf{k}}^{LDA} - E_{v,\mathbf{k}}^{LDA}$ are the band energy differences between $|c, \mathbf{k}\rangle$ and $|v, \mathbf{k}\rangle$ obtained within the GW approximation and that obtained within the LDA, respectively. This approach is known to yield reasonable values for the static dielectric constant of many semiconductors [34].

In our study, we used the generalized gradient approximation [21] to the exchange correlation functional, but the optical matrix elements can be corrected in a similar way to the case of LDA. Therefore, even if we include the many-body effects in the calculation of the optical matrix elements, the effects of spin-orbit coupling on the matrix elements will be small.

We also expect that considering the excitonic effects in our calculations will hardly change our main results. As a result of solving the Bethe-Salpeter equation, an excited state $|S\rangle$ is expanded as $\sum_{\mathbf{k}} \sum_{v}^{\text{hole}} \sum_{c}^{\text{elec}} A_{vc\mathbf{k}}^{S} \hat{a}_{v\mathbf{k}}^{\dagger} \hat{b}_{c\mathbf{k}}^{\dagger} |0\rangle$ [35], where $|0\rangle$ is the many-body ground state and $\hat{a}_{v\mathbf{k}}^{\dagger}$ and $\hat{b}_{v\mathbf{k}}^{\dagger}$ are the creation operators of a hole and an electron, respectively. The optical matrix element that corresponds to the optical excitation from $|0\rangle$ to $|S\rangle$ is given as $\langle 0|\hat{v}|S\rangle = \sum_{\mathbf{k}} \sum_{v}^{\text{hole}} \sum_{c}^{\text{elec}} A_{vc\mathbf{k}}^{S} \langle v, \mathbf{k}|\hat{v}|c, \mathbf{k}\rangle$, which is basically a linear combination of the optical matrix elements, $\langle v, \mathbf{k}|\hat{v}|c, \mathbf{k}\rangle$'s, between single-particle states in the valence and conduction bands that are obtained from DFT calculations. Because our main results on two-dimensional transition-metal dichalcogenides indicate that the effects of spin-orbit coupling on each optical matrix element obtained from DFT calculations are negligible, we expect that the effects of spin-orbit coupling on the optical responses including the excitonic effects will also be small.

Our calculation results show that in studying the optical response of a material with heavy elements, it is sufficient to calculate the optical matrix elements neglecting the commutator arising from spin-orbit coupling in the velocity operator if one has obtained well the electronic structure of the system, i.e., the energy eigenvalues and eigenstates, from fully relativistic first-principles calculations.

[1] C. Jozwiak, C.-H. Park, K. Gotlieb, C. Hwang, D.-H. Lee, S. G. Louie, J. D. Denlinger, C. R. Rotundu, R. J. Birgeneau, Z. Hussain, and A. Lanzara, Photoelectron spin-flipping and texture manipulation in a topological insulator, Nat. Phys. **9**, 293 (2013).

[2] C.-H. Park and S. G. Louie, Spin Polarization of Photoelectrons from Topological Insulators, Phys. Rev. Lett. **109**, 097601 (2012).

[3] J. H. Ryoo and C.-H. Park, Spin-conserving and reversing photoemission from the surface states of Bi_2Se_3 and Au (111), Phys. Rev. B **93**, 085419 (2016).

[4] J. H. Ryoo and C.-H. Park, Momentum-dependent spin selection rule in photoemission with glide symmetry, Phys. Rev. B **98**, 235403 (2018).

[5] Z.-H. Zhu, C. N. Veenstra, G. Levy, A. Ubaldini, P. Syers, N. P. Butch, J. Paglione, M. W. Haverkort, I. S. Elfimov, and A. Damascelli, Layer-by-Layer Entangled Spin-Orbital Texture of the Topological Surface State in Bi_2Se_3, Phys. Rev. Lett. **110**, 216401 (2013).

[6] Z.-H. Zhu, C. N. Veenstra, S. Zhdanovich, M. P. Schneider, T. Okuda, K. Miyamoto, S.-Y. Zhu, H. Namatame, M. Taniguchi, M. W. Haverkort, I. S. Elfimov, and A. Damascelli, Photoelectron Spin-Polarization Control in the Topological Insulator Bi_2Se_3, Phys. Rev. Lett. **112**, 076802 (2014).

[7] B. Adolph, V. I. Gavrilenko, K. Tenelsen, F. Bechstedt, and R. Del Sole, Nonlocality and many-body effects in the optical properties of semiconductors, Phys. Rev. B **53**, 9797 (1996).

[8] A. J. Read and R. J. Needs, Calculation of optical matrix elements with nonlocal pseudopotentials, Phys. Rev. B **44**, 13071 (1991).

[9] S. Baroni and R. Resta, *Ab initio* calculation of the macroscopic dielectric constant in silicon, Phys. Rev. B **33**, 7017 (1986).

[10] A. Marini, G. Onida, and R. Del Sole, Plane-wave DFT-LDA calculation of the electronic structure and absorption spectrum of copper, Phys. Rev. B **64**, 195125 (2001).

[11] Y. Cao, J. A. Waugh, X.-W. Zhang, J.-W. Luo, Q. Wang, T. J. Reber, S. K. Mo, Z. Xu, A. Yang, J. Schneeloch, G. D. Gu, M. Brahlek, N. Bansal, S. Oh, A. Zunger, and D. S. Dessau, Mapping the orbital wavefunction of the surface states in three-dimensional topological insulators, Nat. Phys. **9**, 499 (2013).

[12] C.-Z. Xu, Y. Liu, R. Yukawa, L.-X. Zhang, I. Matsuda, T. Miller, and T.-C. Chiang, Photoemission Circular Dichroism and Spin Polarization of the Topological Surface States in Ultrathin Bi_2Te_3 Films, Phys. Rev. Lett. **115**, 016801 (2015).

[13] L. Kleinman, Relativistic norm-conserving pseudopotential, Phys. Rev. B **21**, 2630 (1980).

[14] J. J. Sakurai and J. Napolitano, *Modern Quantum Mechanics* (Addison-Wesley, Reading, MA, 2011).

[15] G. B. Bachelet, D. R. Hamann, and M. Schlüter, Pseudopotentials that work: From H to Pu, Phys. Rev. B **26**, 4199 (1982).

[16] L. I. Schiff, *Quantum Mechanics* (McGraw-Hill, New York, 1968).

[17] M. S. Hybertsen and S. G. Louie, Spin-orbit splitting in semiconductors and insulators from the *ab initio* pseudopotential, Phys. Rev. B **34**, 2920 (1986).

[18] L. Kleinman and D. M. Bylander, Efficacious form for Model Pseudopotentials, Phys. Rev. Lett. **48**, 1425 (1982).

[19] L. A. Hemstreet, C. Y. Fong, and J. S. Nelson, First-principles calculations of spin-orbit splittings in solids using nonlocal separable pseudopotentials, Phys. Rev. B **47**, 4238 (1993).

[20] G. Theurich and N. A. Hill, Self-consistent treatment of spin-orbit coupling in solids using relativistic fully separable *ab initio* pseudopotentials, Phys. Rev. B **64**, 073106 (2001).

[21] J. P. Perdew, K. Burke, and M. Ernzerhof, Generalized Gradient Approximation Made Simple, Phys. Rev. Lett. **77**, 3865 (1996).

[22] P. Giannozzi, S. Baroni, N. Bonini, M. Calandra, R. Car, C. Cavazzoni, D. Ceresoli, G. L. Chiarotti, M. Cococcioni, I. Dabo, A. Dal Corso, S. de Gironcoli, S. Fabris, G. Fratesi, R. Gebauer, U. Gerstmann, C. Gougoussis, A. Kokalj, M. Lazzeri,

L. Martin-Samos, N. Marzari, F. Mauri, R. Mazzarello, S. Paolini, A. Pasquarello, L. Paulatto, C. Sbraccia, S. Scandolo, G. Sclauzero, A. P. Seitsonen, A. Smogunov, P. Umari, and R. M. Wentzcovitch, QUANTUM ESPRESSO: A modular and open-source software project for quantum simulations of materials, J. Phys.: Condens. Matter **21**, 395502 (2009).

[23] P. Giannozzi, O. Andreussi, T. Brumme, O. Bunau, M. Buongiorno Nardelli, M. Calandra, R. Car, C. Cavazzoni, D. Ceresoli, M. Cococcioni, N. Colonna, I. Carnimeo, A. Dal Corso, S. de Gironcoli, P. Delugas, R. A. DiStasio, Jr., A. Ferretti, A. Floris, G. Fratesi, G. Fugallo, R. Gebauer, U. Gerstmann, F. Giustino, T. Gorni, J. Jia, M. Kawamura, H.-Y. Ko, A. Kokalj, E. Küçükbenli, M. Lazzeri, M. Marsili, N. Marzari, F. Mauri, N. L. Nguyen, H.-V. Nguyen, A. Otero de-la Roza, L. Paulatto, S. Poncé, D. Rocca, R. Sabatini, B. Santra, M. Schlipf, A. P. Seitsonen, A. Smogunov, I. Timrov, T. Thonhauser, P. Umari, N. Vast, X. Wu, and S. Baroni, Advanced capabilities for materials modeling with Quantum ESPRESSO, J. Phys.: Condens. Matter **29**, 465901 (2017).

[24] A. Marini, C. Hogan, M. Grüning, and D. Varsano, Yambo: An *ab initio* tool for excited state calculations, Comput. Phys. Commun. **180**, 1392 (2009).

[25] D. R. Hamann, Optimized norm-conserving Vanderbilt pseudopotentials, Phys. Rev. B **88**, 085117 (2013).

[26] M. Schlipf and F. Gygi, Optimization algorithm for the generation of ONCV pseudopotentials, Comput. Phys. Commun. **196**, 36 (2015).

[27] V. M. Burke and I. P. Grant, The effect of relativity on atomic wave functions, Proc. Phys. Soc. **90**, 297 (1967).

[28] D. J. Griffiths, *Introduction to Quantum Mechanics* (Pearson Prentice Hall, Upper Saddle River, NJ, 2005).

[29] H. J. Monkhorst and J. D. Pack, Special points for Brillouin-zone integrations, Phys. Rev. B **13**, 5188 (1976).

[30] Z. Y. Zhu, Y. C. Cheng, and U. Schwingenschlögl, Giant spin-orbit-induced spin splitting in two-dimensional transition-metal dichalcogenide semiconductors, Phys. Rev. B **84**, 153402 (2011).

[31] M. Gibertini, F. M. D. Pellegrino, N. Marzari, and M. Polini, Spin-resolved optical conductivity of two-dimensional group-VIB transition-metal dichalcogenides, Phys. Rev. B **90**, 245411 (2014).

[32] T. Cao, G. Wang, W. Han, H. Ye, C. Zhu, J. Shi, Q. Niu, P. Tan, E. Wang, B. Liu, and J. Feng, Valley-selective circular dichroism of monolayer molybdenum disulphide, Nat. Commun. **3**, 887 (2012).

[33] Z. H. Levine and D. C. Allan, Linear Optical Response in Silicon and Germanium Including Self-Energy Effects, Phys. Rev. Lett. **63**, 1719 (1989).

[34] R. Del Sole and R. Girlanda, Optical properties of semiconductors within the independent-quasiparticle approximation, Phys. Rev. B **48**, 11789 (1993).

[35] M. Rohlfing and S. G. Louie, Electron-Hole Excitations in Semiconductors and Insulators, Phys. Rev. Lett. **81**, 2312 (1998).